Int J Adv Manuf Technol (2016) 85:209–216
DOI 10.1007/s00170-015-7893-5

ORIGINAL ARTICLE

Optimization of cutter blade profile for face-hobbed spiral bevel gears

Wenchao Guo[1] · **Shimin Mao**[1] · **Yu Yang**[1] · **Yuhua Kuang**[1]

Received: 1 June 2015 / Accepted: 24 September 2015 / Published online: 10 October 2015
© Springer-Verlag London 2015

Abstract To eliminate the tooth edge contact and improve the distribution of the tooth contact stress for face-hobbed spiral bevel gears in the case of heavy load and misalignment considered, optimizing the cutter blade profile is one of the most effective solutions. Generally, a segment of circle arc is used to substitute the straight line to get a desired theoretical tooth contact pattern, however, which is not sufficient for a heavy-loaded gear pair. A multi-segment cutter blade profile with Toprem, Flankrem, and cutter tip is introduced to obtain the ideal load and contact stress distribution. First, the structure of cutter head is described geometrically, the mathematical model of new cutter blade profile is built, and the equation for each section is given in detail. Then, the calculations of all design parameters are represented step by step. Finally, a contrast experiment between the original cutter and new optimal cutter, including tooth contact analysis, finite element analysis, and practical rolling check, is carried out for Oerlikon hypoid gears to verify effectiveness.

Keywords Cutter blade profile · Tooth edge contact · Face-hobbed spiral bevel gears · Tooth contact analysis · Finite element analysis

1 Introduction

Face-hobbed spiral bevel gears are widely used in main drive mechanism of vehicles to transmit power. The face-hobbing method is a continuous indexing method and includes two categories: Klingelnberg and Oerlikon. In recent years, face-hobbed gears attract more and more attention of researchers and users because of their advantages in stability of contact pattern, noise, and strength. A series of achievements have been achieved. A mathematical model of hypoid generator was established by Litvin [1], a mathematical model for universal face-hobbing method was built by Fong and Shih [2], and a tooth topography modification method based on ease-off was also discussed by Fong and Shih [3]. The mathematical model of Klingelnberg cyclo-palloid was also built by Fang [4]. Simon has done a lot of work about face-hobbed gear design and tooth modification based on computer numerical control (CNC) machine: a header cutter with bicircular profile and with optimal diameter was developed in [5], an advanced design method based on the cutter was presented in [6], and the corresponding tooth contact analysis was presented in [7]; polynomial functions were applied to induce variations in the cradle radial setting and the velocity ratio in the kinematic scheme of the machine tool for the generation of the pinion tooth surfaces corresponding to reduced transmission error amplitudes in [8] and [9], a novel method for load distribution calculation is applied to investigate the influence of tooth modifications on loaded tooth contact in [10], and based on [8–10], the optimization methodologies were developed to minimize tooth contact pressures, angular displacement error of driven gear, and transmission error in [11] and [12]; the influence of misalignment on EHD lubrication in face-hobbed spiral bevel gears was discussed in [13], and optimal tooth modifications were presented in [14]; a method which controlled the execution of motions on the CNC hypoid generation using the relations on the cradle-type machine was proposed in [15]. Kawasaki researched the effect of transmission

✉ Shimin Mao
maoshm1@263.net

[1] School of Mechanical Engineering, Xi'an Jiaotong University, Xianning West Road, Xi'an 710049, China

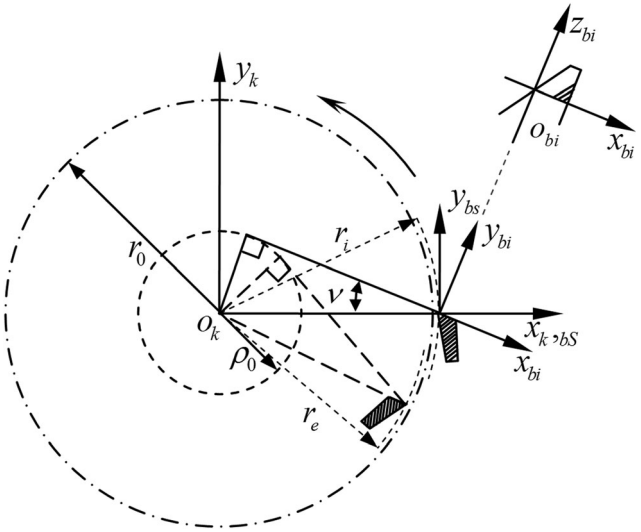

Fig. 1 Description of cutter head geometry

performance by substituting straight cutter blade for arc cutter blade [16, 17]. Fan established the kinematics model of face-hobbing indexing and divided the cutter blade profile into four parts [18]; however, it was not involved on how to divide them. The universal motion concept (UMC) using a cutter head with four-segment blade profile was developed by Fan in [19], and tooth surface error correction was presented based on UMC in [20].

Practice shows that it is likely to generate the tooth edge contact in the case of heavy load, even though the gear design is perfect in theory. To remedy this problem, this paper aims to develop an optimal method of complete cutter blade profile to improve the distribution of tooth contact stress and finite element analysis (FEA) is utilized to verify the feasibility of the method.

2 Modeling of complete cutter blade profile

2.1 Cutter head structure

Generally, cutters for face-hobbed spiral bevel gears are divided into two categories: two-part cutter for Klingelnberg and integral cutter for Oerlikon. Each cutter blade group includes inside blade for cutting tooth convex and outside blade for cutting tooth concave at least.

The geometrical description of left-hand cutter head is shown in Fig. 1. r_0, r_i, r_e are the nominal, inner, and outer radius of cutter head, respectively; ρ_0 is the radius of roll circle, and ν is the lead angle. S_k is the coordinate of cutter head, which is fixed to the cutter head. S_b is the coordinate of cutter blade, an x-axis of which is tangent to the roll circle.

The description of cutter edge profile in S_k is represented by the following matrix equation (based on Fig. 1):

$$\mathbf{r_k}(\mathbf{u}) = \mathbf{M_{kb}}\mathbf{r_b}(\mathbf{u}) \tag{1}$$

The coordinate transformation from S_b to S_k is

$$\mathbf{M_{kb}} = \begin{bmatrix} \cos\nu & \sin(\pm\nu) & 0 & r_{i,e} \\ -\sin(\pm\nu) & \cos\nu & 0 & 0 \\ 0 & 0 & 1 & 0 \\ 0 & 0 & 0 & 1 \end{bmatrix} \tag{2}$$

The upper "+" is used for left-hand cutter, and the lower "–" is used for right-hand cutter.

2.2 Geometry of cutter blade profile

The cutter blade profile of finish cutter is usually composed of circular arc profile and tool nose arc. This type can achieve a good transmission performance and contact pattern when

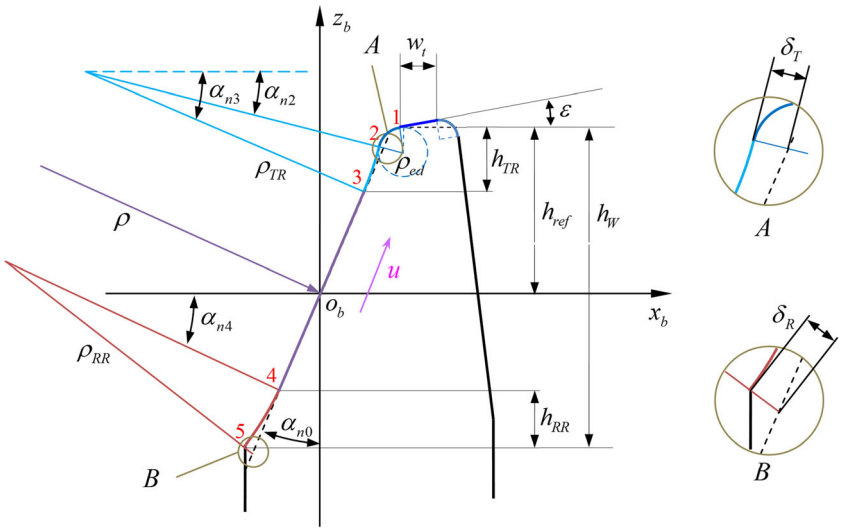

Fig. 2 Description of multi-segment cutter blade profile

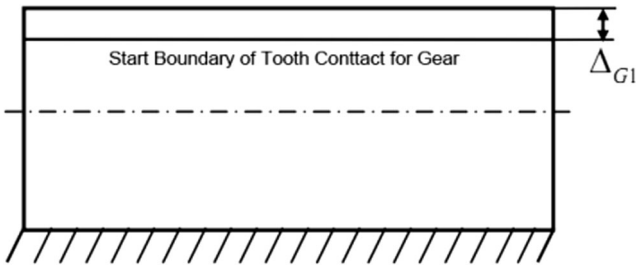

Fig. 3 Start boundary of tooth contact of gear tooth

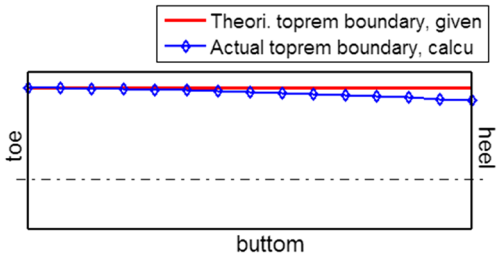

Fig. 5 The theoretical and actual Toprem boundary of pinion tooth

there is no load or light load. However, when there is a heavy load or misalignment, the tooth edge contact (tip-root interference) is likely to happen. A multi-lobe cutter blade profile is introduced to improve this condition in this paper.

As shown in Fig. 2, the multi-segment cutter blade profile consists of five sections: tool nose arc (12), Toprem (23), main profile (34), Flankrem (45), and blade top (16). For convenience, every section is a circular arc except the blade top which is a straight line.

Assuming that u is the parameter of the profile, o_b is the origin; the positive direction is shown in Fig. 2. The equation of each section is shown as follows:

Main profile:

$$\begin{cases} x_B = \rho\left[\cos\left(\alpha_{n0} - u\Big/\rho\right) - \cos\alpha_{n0}\right] \\ z_B = \rho\left[\sin\alpha_{n0} - \sin\left(\alpha_{n0} - u\Big/\rho\right)\right] \end{cases} \tag{3}$$

Toprem:

$$\begin{cases} x_B = \rho(\cos\alpha_{n3} - \cos\alpha_{n0}) + \rho_{TR}(\cos U - \cos\alpha_{n3}) \\ z_B = h_{\mathrm{ref}} - h_{TR} + \rho_{TR}(\sin\alpha_{n3} - \sin U) \\ U = \alpha_{n3} - (u - l_{30})\Big/\rho_{TR} \end{cases} \tag{4}$$

Flankrem:

$$\begin{cases} x_B = \rho(\cos\alpha_{n4} - \cos\alpha_{n0}) + \rho_{RR}(\cos U - \cos\alpha_{n4}) \\ z_B = h_{\mathrm{ref}} + h_{RR} - h_W + \rho_{TR}(\sin\alpha_{n4} - \sin U) \\ U = \alpha_{n4} - (u + l_{40})\Big/\rho_{RR} \end{cases} \tag{5}$$

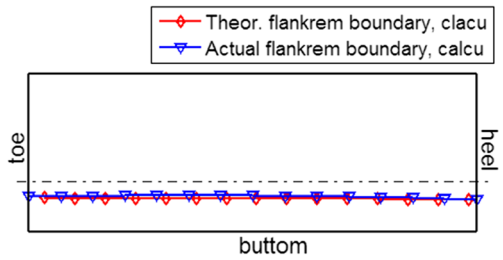

Fig. 4 The theoretical and actual Flankrem boundary of pinion tooth

Tool nose arc:

$$\begin{cases} x_B = \rho(\cos\alpha_{n3} - \cos\alpha_{n0}) + \rho_{\mathrm{ed}}\cos\alpha_{n2} \\ \quad + \rho_{TR}(\cos\alpha_{n2} - \cos\alpha_{n3}) - \rho_{\mathrm{ed}}\cos U \\ z_B = h_{\mathrm{ref}} - \rho_{\mathrm{ed}} + \rho_{\mathrm{ed}}\sin U \\ U = \alpha_{n2} + (u - l_{23} - l_{30})\Big/\rho_{\mathrm{ed}} \end{cases} \tag{6}$$

where l_{ij} is the arc length of each section and α_{ni} is the profile angle of each point. All of them can be acquired through sample calculation.

3 Design of cutter blade profile

As shown in Fig. 2, the cutter blade profile will be determined, if we get the following values: blade profile angle (α_{n0}), reference height (h_{ref}), profile curvature radius (ρ), Toprem height (h_{TR}), Toprem curvature radius (ρ_{TR}), Flankrem height (h_{RR}), Flankrem curvature radius (ρ_{RR}), edge radius (ρ_{ed}), blade top width (w_{t}), and blade top slope angle (ε). How to determine them is called the design of cutter blade profile.

Generally, h_{ref} depends on tooth reference point and tooth height and ρ is calculated by tooth contact analysis (TCA), so both of them are not introduced in this paper. The calculation

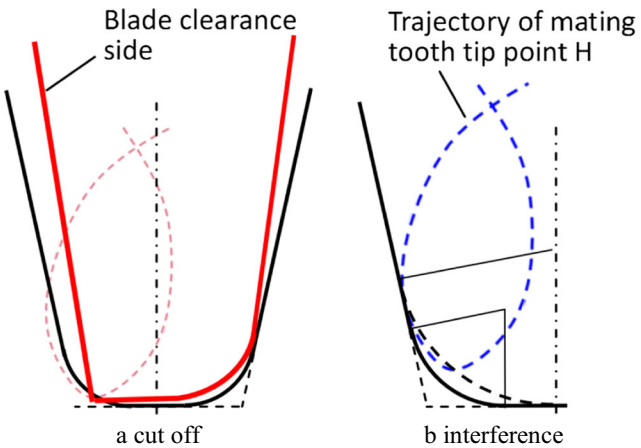

Fig. 6 Blade tip cutoff (**a**) and tooth tip interference (**b**)

Table 1 Gear pair data

	Pinion	Gear
Shaft angle (°)/offset (mm)	90/30	
Number of teeth	10	37
Module (mm)	–	12.703
Face width (mm)	65.48	60.00
Pitch cone angle (°)	18.9245	76.9537
Mean spiral angle (°)	43.7767	35
Mean cone distance (mm)	186.12	210.95

of others will be discussed in detail. The steps will be represented by taking the cutter blade profile for pinion as an example.

First, by assuming that the gear (wheel) tooth without modification and the profile curvature radius of pinion blade are known, the concrete steps are undertaken as follows:

(a) *Define the start boundary of tooth contact for gear*. The start boundary of tooth contact is a straight line which is parallel to the tooth tip. As shown in Fig. 3, Δ_{G1} is the distance from the start boundary to the tooth tip in the gear tooth.

(b) *Calculate the theoretical Toprem boundary for pinion*. The theoretical Toprem boundary is a point set composed of the pinion tooth points which mesh with the start boundary given in (a). Consequently, this step needs the meshing function of gear pair. The boundary is the line with diamonds (red) in Fig. 4.

(c) *Calculate the Toprem height* (h_{TR}). First is to calculate u sets composed of surface parameter u of each point in the theoretical Toprem boundary, and their calculations need the meshing function between pinion and the generating crown gear. Then, minimum $u_{\min}$ can be decided. Its locus is the actual Toprem boundary, which is the line with inverted triangles (blue) in Fig. 4. h_{TR} is the distance from point $u_{\min}$ to blade tip when ε=0.

(d) *Calculate the Flankrem height* (h_{RR}). First is to select the start boundary in pinion tooth as (a), second is to calculate the u sets according to the theoretical Flankrem boundary (Fig. 5) as (c), and then maximum $u_{\max}$ can be decided. Its locus is the actual Flankrem boundary in Fig. 5. h_{RR} is the distance from the point $u_{\max}$ to the blade root. It is worth noting that all elements of u sets in this step are negative.

Table 2 Machine settings

	Pinion	Gear
Tilt angle (°)	20.39	0
Swivel angle (°)	325.310	0
Radial distance (mm)	247.286	0
Vertical (mm)	–	183.901
Horizontal (mm)	–	172.422
Work offset (mm)	30.586	0
Mach center to cross point (mm)	−0.2948	0
Sliding base (mm)	46.644	0
Machine root angle (°)	−0.4	70.890
Ratio of roll	3.69776	–
Center roll position (°)	54.42	0

Table 3 Original cutter data

	Pinion cutter		Gear cutter	
	Outside	Inside	Outside	Inside
Number of blade groups	17		17	
Cutter radius (mm)	174.056	174.741	174.056	174.741
Blade flank angle (°)	25.415	21.55	25.415	21.55
Lead angle (°)	26.569	26.457	26.569	26.457
Axial grind depth (mm)	22.12	22.12	22.12	22.12
Reference height (mm)	11.087	11.592	11.087	11.592
Radius curvature (mm)	1500	1500	1500	1500
Edge radius (mm)	1.2	1.2	1.2	1.2
Blade top width (mm)	1.14	1.14	1.14	1.14
Edge radius, clear (mm)	0.8	0.1	0.8	0.1

Table 4 New optimal cutter data

	Pinion cutter		Gear cutter	
	Outside	Inside	Outside	Inside
Number of blade groups	17		17	
Cutter radius (mm)	174.056	174.741	175.464	174.282
Blade flank angle (°)	25.415	21.55	25.212	21.973
Lead angle (°)	26.569	26.457	26.339	26.534
Axial grind depth (mm)	22.12	22.12	22.124	22.124
Reference height (mm)	11	11.592	11.35	11.35
Radius curvature (mm)	1500	1500	1500	1500
Toprem height (mm)	4.37	4.64	9.65	4.99
Toprem radius (mm)	40	42	246	30
Toprem value (mm)	0.15	0.15	0.15	0.15
Flankrem height (mm)	7.02	6.39	–	–
Flankrem radius (mm)	72	53	–	–
Flankrem value (mm)	0.25	0.25	–	–
Edge radius (mm)	1.8	1.8	3.0	3.0
Blade top width (mm)	0.5	0.8	2.1	2.1
Top slope angle (°)	3.0	−3.0	0	0
Edge radius, clear (mm)	1.0	1.0	1.5	1.5

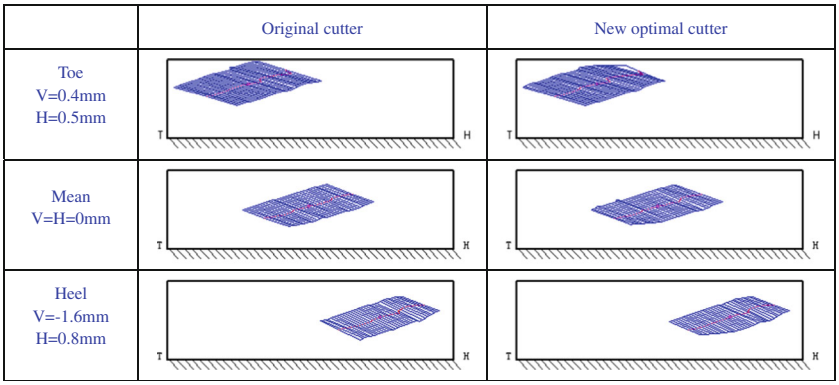

Fig. 7 Tooth contact patterns corresponding to original and new optimal cutter

(e) *Calculate the curvature radius* (ρ_{TR} and ρ_{RR}). Toprem curvature radius (ρ_{TR}) is calculated according to the condition of tangential contact and the given value δ_T at point 2. Similarly, Flankrem curvature radius (ρ_{RR}) can be derived according to the condition of tangential contact and the given value δ_R at point 4.

(f) *Decide the blade edge radius* (ρ_{ed}). The edge radius (ρ_{ed}) cannot be calculated directly, which is influenced by the blade top width (w_t) and the top slope angle (ε). Therefore, the value of ρ_{ed} is selected using a trial and error method. However, there are two rules must be observed:

1. Choose the maximum value without excessive cutoff (Fig. 6a)
2. Choose the maximum value without interference between the tooth transition surface and the trajectory of matching tooth flank tip (Fig. 6b).

Although the above calculations are quite complicated, if the value Δ_{G1}, δ_{TP}, and δ_{RP} are given, the pinion cutter blade profile could be determined. Similarly, for gear cutter, the value Δ_{G1}, δ_{TP}, and δ_{RP} are needed.

4 Experiment study

In this section, tooth contact analysis (TCA), finite element analysis (FEA), and rolling check were carried out on a pair of hypoid gears manufactured using a Oerlikon "Spirac" method.

4.1 Gear pair and cutter data

The data of the hypoid gears, machine settings, and original cutter are all presented in Tables 1, 2, and 3. The configurations of control parameters are decided using a trial and error method. The new optimal cutter data calculated using the above method are presented in details in Table 4.

4.2 Tooth contact analysis

With the machine settings and cutter data listed in above tables, tooth surface points of pinion and mating gear could be derived from computer program based on the mathematic model presented in [2]. Then, TCA can be done using the coordinate, normal, and curvature parameters of tooth surface point and the tooth contact patterns of the hypoid gear pair manufactured using original cutters and the new optimal cutters are listed in Fig. 7.

As shown in Fig. 7, tooth contact patterns which located in the toe, mean, and heel, respectively, are illustrated and their *V*–*H* values are also labeled. The left column of the contact patterns is corresponding to the original cutter, and the right is to the new optimal cutter. From the pictures, we can see that the shapes of contact patterns to the original cutter are all diamond rhombus with sharp corners and the patterns corresponding to the new cutter are similar. However, when the corner of the pattern gets close to the tip or root, it will be changed like chamfering and not a sharp corner at all (toe and heel). That is to say, the new cutter could avoid the tip-root contact effectively. From the figures, we can also see that the

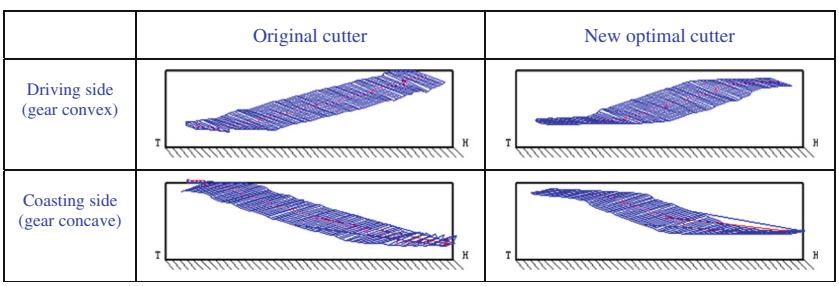

Fig. 8 Tooth contact patterns for single tooth meshing corresponding to original and new optimal cutter

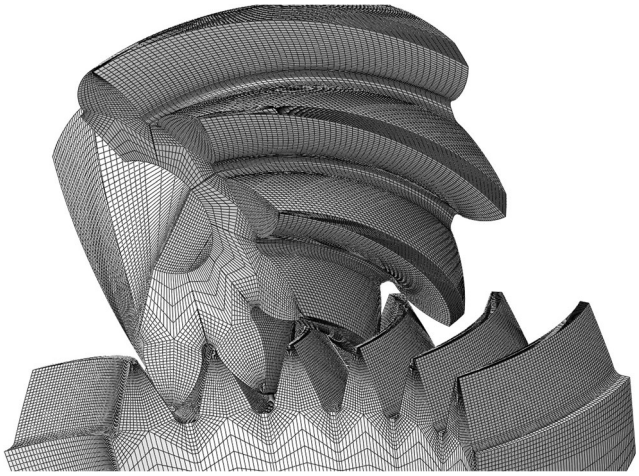

Fig. 9 The six-tooth FEA model of hypoid gears

sizes and positions of the contact patterns corresponding to the two cutters always are identical whenever they are in the toe, mean, or heel. In others words, the new optimal cutter does not change the position of the tooth contact pattern.

The complete tooth contact pattern for the single tooth meshing (without considering tooth contact ratio) is shown in Fig. 8. Similar to Fig. 7, the left column corresponds to the original cutter and the right corresponds to the new optimal cutter. Figure 8 visually shows that the tooth edge contact occurred in both driving and coasting side for the left column but did not occur in the right column. Thus, it can be seen that this blade profile optimal method does improve the distribution of tooth contact stress indeed.

In a word, the new cutter could avoid the tooth edge contact validly without influencing the tooth contact pattern's position and size.

4.3 Finite element analysis

In order to ensure the accuracy of the finite element analysis, a new model method which treats the actual tooth surface points as element's nodes is introduced in this paper. This method can avoid nodes' errors resulting from modeling, especially in the tip of pinion tooth flank and transition surface.

The FEA model can be built using the above modeling method. According to the convergence analysis, a grid of (25+9)×61 is chosen, which means that there are 25 nodes for tooth flank and 9 nodes for transition surface in the direction of tooth height and 61 nodes in the direction of face width. The six-tooth FEA model is shown in Fig. 9.

A group of the misalignment (E=−0.3641 mm, p=0.3498 mm, G=0.0133 mm, A=0.0327°) was used, which was derived from the test bed by measuring in the case of a heavy load of 30,000 Nm. The two groups of FEA for driving side were carried out through the Abaqus software at the same conditions, respectively, and each group was composed of 20 continuous positions for a complete meshing process of one tooth. The FEA results of the 15th position for original cutter and new optimal cutter are shown in Fig. 10.

The figures about original cutter show that the maximum tooth contact stress occurs in tooth tip or root for each position, the maximum stress is up to 2527 MPa in pinion tooth and 2212 MPa in gear tooth. The pictures about new cutter indicate that all maximum stresses for optimal cutter occur in the inner of tooth flank; the maximum stress is 1927 MPa in pinion tooth and 2014 MPa in gear tooth. Comparing two groups of FEA results, we can get that the new cutter greatly improves the distribution of tooth contact stress, eliminates the tooth edge contact, and decreases the maximum stress observably.

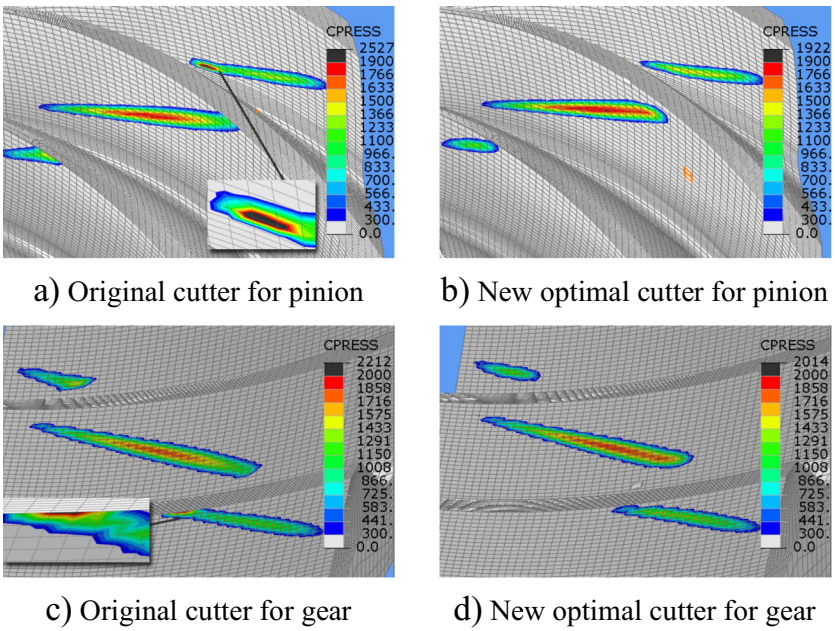

Fig. 10 **a**–**d** FEA results for original and new optimal cutters

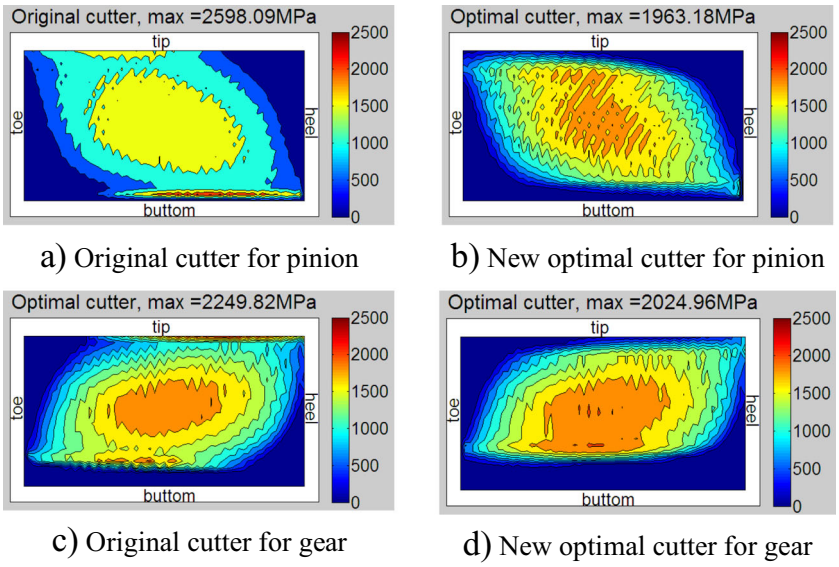

Fig. 11 **a**–**d** Color nephograms of maximum contact stress

The color nephograms of contact stress (Fig. 11) also were made out according to the maximum stress of each node in the 20 positions to explain the distribution of contact stress in the total meshing process. Figure 11 visually describes that the new optimal cutter avoided the tip-root contact effectively and reduced the maximum contact stress observably without changing the desired tooth contact pattern. The rate of decrease is up to 24.44 % (from 2598.09 to 1963.18) in the pinion tooth and also 9.99 % (from 2249.82 to 2024.96) in the matching gear tooth.

4.4 Rolling check

The cutting and rolling test experiments were carried out to validate this method further. The new optimal cutter blades were grinded using the Gleason BPG grinding machine, and the hypoid gears were cut using the Gleason Phoenix II 600HC milling machine. In order to compare the theoretical TCA contact patterns conveniently, the same values of *V*–*H* were used during the rolling check and the corresponding results are shown in Fig. 12.

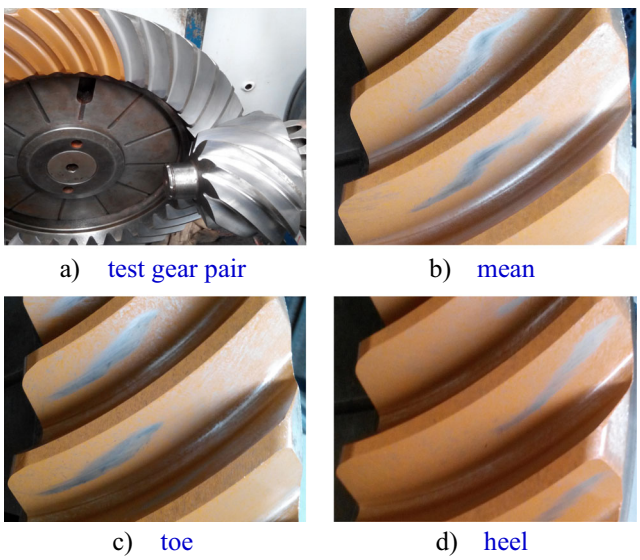

Fig. 12 **a**–**d** Tooth contact patterns of rolling check

The hypoid gears manufactured using new cutters and used to rolling check are shown in Fig. 12a, and rolling check contact patterns lengthwise located in the mean, toe, and heel along the tooth are shown in Fig. 12b–d, respectively. Comparing with the TCA results shown in Fig. 7 (right column), there were little differences between the real contact patterns and the theoretical ones: the real contact pattern in Fig. 12b becomes a little close to the toe relative to the theoretical one, and the real contact pattern in Fig. 12c moves a little to the root. Nevertheless, the position, size, and shape of the real contact patterns and the theoretical ones were very consistent on the whole. The rolling results validated the effectiveness of the new optimal method in practice again.

5 Conclusion

This paper discusses an optimal design method of cutter blade profile for face-hobbed spiral bevel gears, which is a multi-segment composed of five sections. The formula of each section and the calculation method (or rules) of unknown parameters are given in detail. The theoretical comparison of tooth contact patterns by TCA between the new optimal cutter and original cutter is carried out. An accuracy gear FEA modeling method which treats tooth surface points as element's nodes is also described. The FEA results in the case of heavy load indicate that the method could avoid or eliminate the tooth edge contact effectively and decrease the maximum tooth

contact stress observably. This method can also be applied to other rotary cutters directly.

Acknowledgments The authors are grateful to the National Key S&T Special Projects for their financially supporting.

References

1. Litvin FL, Chaing WS, Kuan C, Lundy M, Tsung WJ (1991) Generation and geometry of hypoid gear-member with face-hobbed teeth of uniform depth. Int J Mach Tools Manuf 31:167–181
2. Shih YP, Fong ZH, Lin GC (2007) Mathematical model for a universal face hobbing hypoid gear generator. J Mech Des 129:38–47
3. Shih YP, Fong ZH (2007) Flank modification methodology for face-hobbing hypoid gears based on ease-off topography. J Mech Des 129:294–302
4. Du JF, Fang ZD, Xu M, Zhao XL, Feng YM (2013) Mathematical model of Klingelnberg cyclo-palloid hypoid gear. Energy Res Power Eng 341–342:572–576
5. Simon V (2009) Head-cutter for optimal tooth modifications in spiral bevel gears. Mech Mach Theory 44(7):1420–1435
6. Simon V (2009) Advanced design and manufacture of face-hobbed spiral bevel gears. In ASME 2009 International Mechanical Engineering Congress and Exposition, pp. 539-548. American Society of Mechanical Engineers.
7. Simon V (2011) Generation and tooth contact analysis of face-hobbed spiral bevel gears. Chin J Aeronaut 25:A9–A288
8. Simon VV (2010) Advanced manufacture of spiral bevel gears on CNC hypoid generating machine. J Mech Des 132(3):031001
9. Simon VV (2011) Generation of hypoid gears on CNC hypoid generator. J Mech Des 133(12):121003
10. Simon V V (2011) Influence of tooth modifications on load distribution in face-hobbed spiral bevel gears. In ASME 2011 International Design Engineering Technical Conferences and Computers and Information in Engineering Conference, pp. 135-147. American Society of Mechanical Engineers.
11. Simon VV (2014) Optimal machine-tool settings for the manufacture of face-hobbed spiral bevel gears. J Mech Des 136(8):081004
12. Simon V (2013) Design of face-hobbed spiral bevel gears with reduced maximum tooth contact pressure and transmission errors. Chin J Aeronaut 26(3):777–790
13. Simon V V (2013) Minimization of the influence of misalignments on EHD lubrication in face-hobbed spiral bevel gears. In ASME 2013 International Design Engineering Technical Conferences and Computers and Information in Engineering Conference, pp. V005T11A037-V005T11A037. American Society of Mechanical Engineers.
14. Simon VV (2014) Optimal tooth modifications in face-hobbed spiral bevel gears to reduce the influence of misalignments on elastohydrodynamic lubrication. J Mech Des 136(7):071007
15. Simon VV (2014) Manufacture of optimized face-hobbed spiral bevel gears on computer numerical control hypoid generator. J Manuf Sci Eng 136(3):031008
16. Kawasaki K (2007) Effect of cutter blade profile on meshing and contact of spiral bevel gears in cyclo-palloid system. Mech Based Des Struct Mach Int J 33:343–357
17. Kawasaki K, Tsuji I(2009) Analytical and experimental tooth contact pattern of large-sized spiral bevel gears in cyclo-palloid system. ASME 2009 International Design Engineering Technical Conferences and Computers and Information in Engineering Conference, pp. 139-47
18. Fan Q (2006) Kinematical simulation of face hobbing indexing and tooth surface generation of spiral bevel and hypoid gears. Gear Technol 23(1):30–38
19. Fan Q (2007) Enhanced algorithms of contact simulation for hypoid gear drives produced by face-milling and face-hobbing processes. J Mech Des 129(1):31–37
20. Fan Q (2010) Tooth surface error correction for face-hobbed hypoid gears. J Mech Des 132(1):011004